Journal of Applied Physics ARTICLE scitation.org/journal/jap

Controlled generation of photoemissive defects in 4H-SiC using swift heavy ion irradiation

Cite as: J. Appl. Phys. **129**, 245905 (2021); doi: 10.1063/5.0051328
Submitted: 24 March 2021 · Accepted: 13 June 2021 ·
Published Online: 30 June 2021

Anusmita Chakravorty,[a] Budhi Singh, Hemant Jatav, Ramcharan Meena, D. Kanjilal, and D. Kabiraj[b]

AFFILIATIONS

Inter-University Accelerator Centre, Aruna Asaf Ali Marg, New Delhi 110067, India

[a]**Electronic mail:** anusmitachakravorty@iuac.res.in
[b]**Author to whom correspondence should be addressed:** kabiraj@iuac.res.in

ABSTRACT

Defects in SiC have shown tremendous capabilities for quantum technology-based applications, making it necessary to achieve on-demand, high-concentration, and uniform-density defect ensembles. Here, we utilize 100 MeV Ag swift heavy ion irradiation on n-type and semi-insulating 4H-SiC for the controlled generation of the defects that have attracted a lot of attention. Photoluminescence spectroscopy shows strong evidence of V_{Si} emitters in semi-insulating 4H-SiC. Additionally, irradiation generates photo-absorbing centers that enhance the optical absorption, suppressing the luminescence intensity at higher fluences (ions/cm^2). In n-type 4H-SiC, irradiation drastically increases the inter-conduction band transitions, attributed to absorption from trap centers. A clear correlation is found between (i) loss in the intensity of E_2 (TO) Raman signal and the enhancement in absorbance at 532 nm and (ii) decoupling of the longitudinal optical phonon–plasmon coupled Raman mode and the reduction in carrier concentration. The optical bandgap decreases with irradiation fluence for semi-insulating 4H-SiC. This is attributed to the formation of disorder and strain-induced localized electronic states near the band edges.

I. INTRODUCTION

4H-SiC has evolved as a promising substitute for traditional semiconductors owing to its structural, chemical, and mechanical stability.[1] With the progression in materials development and expanding level of refinement in wafer growth technology, point defects, dopants, contaminations, and structural imperfections have become urgent issues inside the SiC research groups. Further, a few of these issues are not only exclusively connected to the materials development but also to the processes utilized for device fabrication like oxidation, doping by particle implantation, ohmic-contact formation, and surface passivation.[2] Prompted by the potential applications of SiC in harsh environments, such as in the aerospace, aviation, and nuclear reactor fields, where high-temperature and high-radiation conditions are involved, experimental and theoretical efforts have been made for the development of better understanding of the radiation-damage processes.[3,4] Besides, ion implantation required for device fabrication introduces defects that often kill the carrier lifetime and limit the device operations. Furthermore, the 100 MeV Ag ions used for irradiation in this study replicate the conditions due to the fission fragments emitted in nuclear fission and cosmic radiation. Thus, the results will be useful for predicting device performances under such a radiation environment. The different point defects in SiC that are extensively studied include silicon vacancy (V_{Si}), carbon vacancy (V_C), carbon interstitial (C_I), silicon interstitial (Si_I), and antisite defects (C_{Si} and Si_C).[2] Various defects that SiC can host hold great importance in the field of quantum science.[5–13] Recent research efforts have established that V_{Si} in SiC is a promising defect center for single defect-based qubits and quantum sensing applications.[12–17] Various practical applications demand the generation of V_{Si} with high efficiency. The energetic particle induced binary collision process is the only possible route to generate these defects in a controlled manner. It has been experimentally demonstrated that V_{Si} can be produced in SiC after bombardments with protons, electrons, and ion beams (He, C, and Si).[12,14,18,19] Recently, high conversion efficiency exhibited by the V_{Si} defects in 4H-SiC after 20 keV He irradiation has paved the way for the production of high concentration defect ensembles.[19] Previously performed low energy ion implantations led to a non-uniform defect distribution, extending to a range not exceeding ~300 nm. It is important to generate efficiently high-concentration and uniform-density defect ensembles extending to micrometer depths to enhance the sensitivity in

applications. The uniform concentration and distribution provides a larger area with equal efficiency to be used for applications. It also removes any ambiguity related to the position of the defect when the material is integrated for quantum applications. After the scientific evidence for nitrogen-vacancy (NV) centers in diamond as a single-photon source, extensive research has been carried out for uniform creation of vacancies through the volume of the sample, controlling the concentrations as well as their spatial localization within the diamond.[20] In particular, precisely controlling NVs density in the crystal as well as their close environment is crucial to achieving optimal spin properties for quantum sensing applications.[20,21] In this work, we attempt to create a $\sim 5\,\mu$m thick uniformly defective layer in 4H-SiC that provides a method to create a uniform environment for the generated vacancies.

In this paper, the novel energy loss process of swift heavy ions (SHIs) has been used to facilitate the production of uniform defect concentration within several micrometers of the sample. Irradiation parameters such as the ion range and stopping power corresponding to the ion energy have been calculated by using the transport of ions in matter (TRIM) 2013 full-cascade simulations.[22] From the depth profiles of elastic energy loss (S_n) due to 100 MeV Ag in SiC [Fig. 1(a)], it can be noted that the energy lost by the incoming ion that is transferred to the recoiling target nucleus is almost uniform within a window of about 5 μm from the sample surface, indicating modification of a substantial volume of the material. This S_n is responsible for the production of defect density ranging from 1×10^{19} to 5×10^{20} vacancies/cm^3 within this window, as shown in Fig. 1(b). The value of S_n is low, so presumably, the generated defects are primarily point defects. Moreover, the high-energy ions ensure low angle scattering with the target atoms and helps us in retaining the collision events close to the almost undistorted ion trajectory. A transverse view of the collision events is plotted using the TRIM generated file named COLLISON.txt that contains the data on every ion/target collision [Fig. 1(c)]. This confirms that the scattering events occur in the neighborhood of the ion trajectory. Further, the simulation indicates that the primary knock-on events within a single trajectory remain spatially separated, preventing the secondary cascade overlaps if produced. Results indicate that photo-emission reduces after the fluence of 5×10^{12} ions/cm^2. At this fluence, the radius of the zone of inter-track interaction can be estimated as $\sim$2.5 nm. Thus, inter-trajectory interaction between defects to form complexes can be controlled. Recently, it was shown that the intense ionizing energy deposited by 100 MeV Ag ions does not lead to any drastic structural modifications in 4H-SiC.[23] The interest of this work lies in the determination of the modifications induced in the low structural damage regime for which point defects are prevalent. Investigations were performed with methods such as photoluminescence (PL) spectroscopy, confocal Raman spectroscopy, UV-vis absorption spectroscopy, and Hall measurements. Both nitrogen-doped (n-type) and semi-insulating (SI) 4H-SiC single crystals irradiated under identical conditions are analyzed to study the modifications in the optical and electronic structure. The V_C defects are unavoidably present even in the best in class epitaxially grown 4H-SiC and act as a "killer" for the free carriers.[24,25] This experimental effort presents a method for the generation and detection of the more challenging V_{Si} in the bandgap. The combined experimental results from both

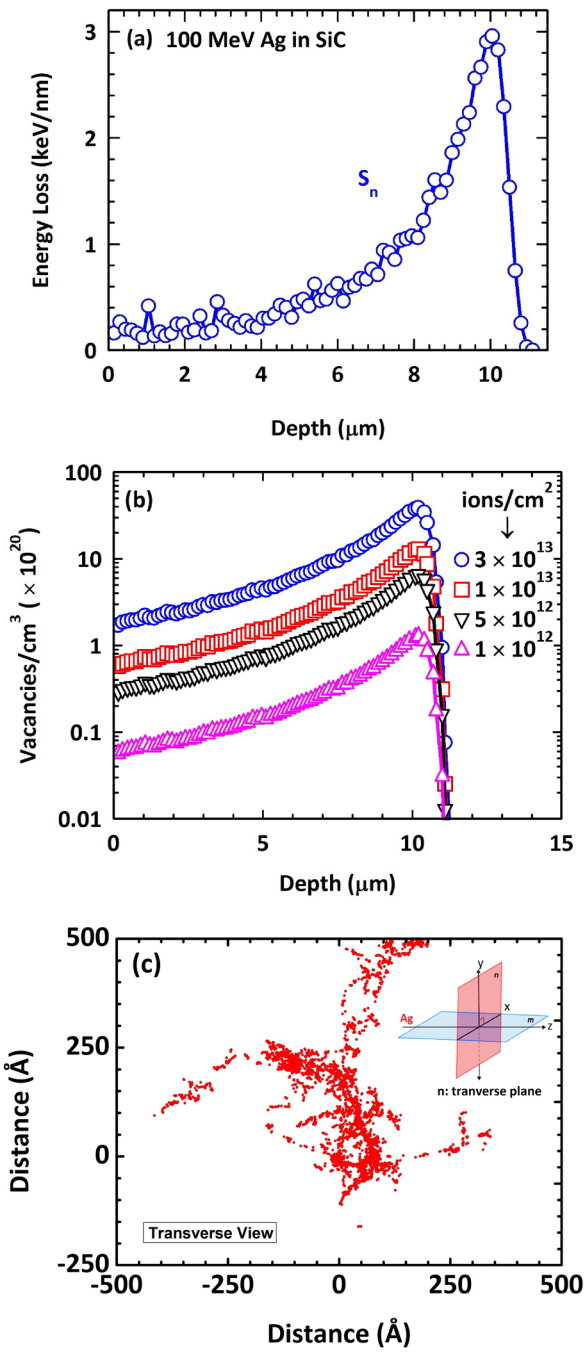

FIG. 1. (a) The depth profile of elastic energy loss in SiC irradiated with 100 MeV Ag ions simulated with the TRIM 2013 code.[22] (b) The variation of vacancies with depth as estimated using TRIM simulation for different Ag ion fluences. The units of indicated ion fluences are in (ions/cm^2). (c) TRIM simulated transverse view of single ion generated collision cascades. Inset to (c) represents the ion trajectory along the Z-direction and X–Y plane (*n*) is the transverse plane that is perpendicular to the ion trajectory. The coordinates X = 0 and Y = 0 represent the intersection of the ion's path with *n*.

sample types used in this study indicate that due to irradiation, there is a formation of tail states in the bandgap, which is responsible for a decrease in the bandgap energy and the enhanced inter-band transitions. The irradiation leads to enhancement of inter-band transition as compared to the below bandgap absorption, and quenching of the free carriers in n-type 4H-SiC, predicting the generation and enhancement of electron trap-like defects.

II. EXPERIMENTS

The n-type and SI 4H-SiC ⟨0001⟩ single-crystal wafers were procured from Semiconductor Wafer Inc., Taiwan. The wafer was diced into pieces of dimension $1 \times 1\,cm^2$ for experimental purposes. The samples were subjected to irradiation with 100 MeV Ag at various fluences (1×10^{12}–6×10^{13} ions/cm^2) using the 15-UD Pelletron accelerator facility at the Inter-University Accelerator Centre in New Delhi, India.[26] Irradiations were carried out at room temperature with an ion current maintained at 1 particle nanoampere (pnA, $1\,pnA = 6.25 \times 10^9$ ions/s) to avoid excessive heating of the targets. To avoid ion channeling, the normal to the sample surface was tilted by 7° to the incident beam direction. An excitation wavelength of 532 nm from Nd:YAG laser was used for performing Raman spectroscopy using the WITec GmbH Raman microscope equipped with a 100× objective lens and a numerical aperture of 0.9. The laser was focused on a $1 \times 1\,\mu m^2$ region and the power was adjusted to around 150 mW to avoid heating effects. The absorption spectra were recorded using the Hitachi U-3300 spectrophotometer in the 200–650 nm wavelength range with a spectral resolution of 0.2 nm. The electrical properties of the samples were measured by the Ecopia HMS-3000 Hall measurement system using a 0.5 T magnetic field. For performing the Hall measurements, ohmic contacts were fabricated in the four corners of the samples (Van der Pauw geometry). Prior to irradiation, ohmic contacts were made to avoid defect annealing during thermal treatment. Nickel (60 nm thick) and gold (40 nm thick) contacts were deposited consecutively by thermal evaporation under high vacuum conditions. This was followed by annealing at 950 C for 2 min under flowing Ar gas in a tubular furnace. PL measurements were performed at 77 K using a 266 nm deep UV excitation from the Crylas FQCW-266-series laser system exciting with a power of 40 mW. The front surface excitation of the samples emitted radiation, which was collected for PL spectroscopy. The PL signal was focused at the entrance slit of Jovin Yvon Triax 550 monochromator and dispersed with a grating of 600 g/mm. A Peltier cooled Si detector placed at the exit port of the monochromator with a hemispherical light concentrator was used to detect light signals. The PL data were recorded using the lock-in technique with a mechanical chopper. Appropriate long pass filters were used to collect data in the ranges of 350–600 nm and 850–1150 nm. The implanted ions are deep inside the material and thus do not interfere in the measurements except for optical absorption spectroscopy because it involves the entire thickness of the sample. The wavelength of the excitation light used for performing Raman has a penetration depth of ∼2 mm in 4H-SiC but utilizing the confocal Raman arrangement allowed information only from a depth about 2 μm to reach the detector. The PL measurements were performed by ultraviolet light having a very shallow penetration depth of ∼250 nm but the probing depth of PL may further be suppressed by surface recombinations and trapping of photo-excited carriers by non-radiative channels.

III. RESULTS AND DISCUSSION

A. Photoluminescence spectroscopy

There are two different kinds of vacancies and inequivalent sites in 4H-SiC, V_{Si} and V_C at cubic (k) and hexagonal (h) sites.[27] The substitution of impurities and point defects at two inequivalent substitutional sites makes PL spectra of 4H-SiC complicated.[28] The PL observed for n-type 4H-SiC further becomes quite complex and involves several other unrecognized defect complexes, making it difficult to isolate transitions due to the native defects (V_C and V_{Si}) that are recognized from the experiments. Moreover, the generation rate of Frenkel-pairs does not depend on the conduction-type in SiC.[29] Thus, recording the spectra of the SI sample enabled us to eliminate the contributions from nitrogen-vacancy centers, which produce near-infrared luminescence.[30] However, impurities like N, B, and Al that are incorporated even during nondoped growth give rise to an unavoidable luminescence. In Figs. 2(a) and 2(b), PL spectra recorded before and after irradiation in SI 4H-SiC with various fluences are shown. In the range 350–600 nm, the pristine sample exhibits two broad bands: (i) a signal including the "near band edge" emission and the D1 PL band[31] and (ii) an intense sideband with a peak centered around 505 nm. The Si antisite (Si_C) defect has been assigned as the defect responsible for the D1 PL.[32,33] The broadband at 505 nm has been attributed to V_C (Si–Si dimmers) surface defects in SiC.[34,35] This broad green feature has also been ascribed to vacancies of carbon and its extended point defects in unintentionally doped 4H-SiC homoepitaxial layers.[36] The most probable recombination path for this PL is often associated with donor–acceptor pairs (DAPs) of nitrogen with a structural defect.[37] This defect-related PL was studied by Lebedev *et al.* after electron irradiation on n-type 4H-SiC doped with various nitrogen concentrations.[38] It was concluded that the concentration of DAPs is characteristic of the given growth procedure and is independent of the carrier concentration. Interestingly, some p-type samples also demonstrated the appearance of this feature.[39] It was found that despite having all the nitrogen impurities compensated by acceptor type doping, the DAP intensity in the p-type sample enhanced after irradiation with 15 MeV proton.[39] Cathodoluminescence studies performed on SHI (167 MeV Xe) irradiated n-type 4H-SiC also exhibited a similar broad spectral band whose intensity reduced substantially after irradiation.[40] The decrease in intensity was attributed to (i) radiation-accelerated defect diffusion and (ii) radiation defect induced gettering of structural imperfections in 4H-SiC.[40–46] In our results, the DAP intensity was found to decrease with fluence, supporting previously observed behavior after SHI irradiation. Furthermore, PL measurements were performed in the range of 850–1150 nm to enable detection of the V_{Si} defect generated after SHI irradiation. The irradiated samples showed features related to V_{Si} along with a number of defect centers of unknown origin (UD_4 and UD_3) that are reported previously.[12–14,18,19,47,48] In 4H-SiC, the V_{Si} transitions originate from internal transitions between the ground and the excited multiplet-states of V_{Si}^{-1}(k) and V_{Si}^{-1} (h).[49] As noticed, for the SHI irradiated samples, the

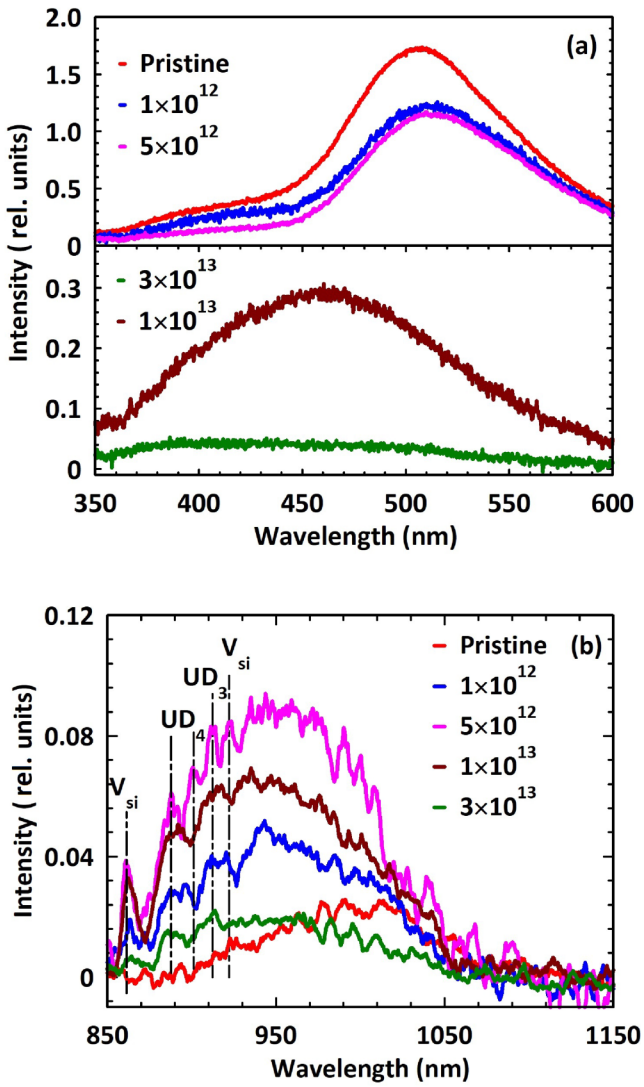

FIG. 2. Photoluminescence spectra recorded before and after 100 MeV Ag irradiation in semi-insulating 4H-SiC with various fluences (ions/cm^2). Recording ranges: (a) 350–600 nm and (b) 850–1150 nm.

PL intensity increases as the irradiation fluence is increased to 5×10^{12} ions/cm^2, suggesting an expansion in the number of defect states. However, beyond this fluence, the intensity decreases, which means that it has an optimal irradiation fluence. At the highest irradiation fluence, the PL intensity was observed to drop significantly due to the non-radiative transitions as supported by enhanced absorption due to the generation of photo-absorbing defect centers.

B. Raman spectroscopy and Hall measurements

Raman spectroscopy studies were carried out to extract details about the composition and chemical disordering. Figure 3(a) shows

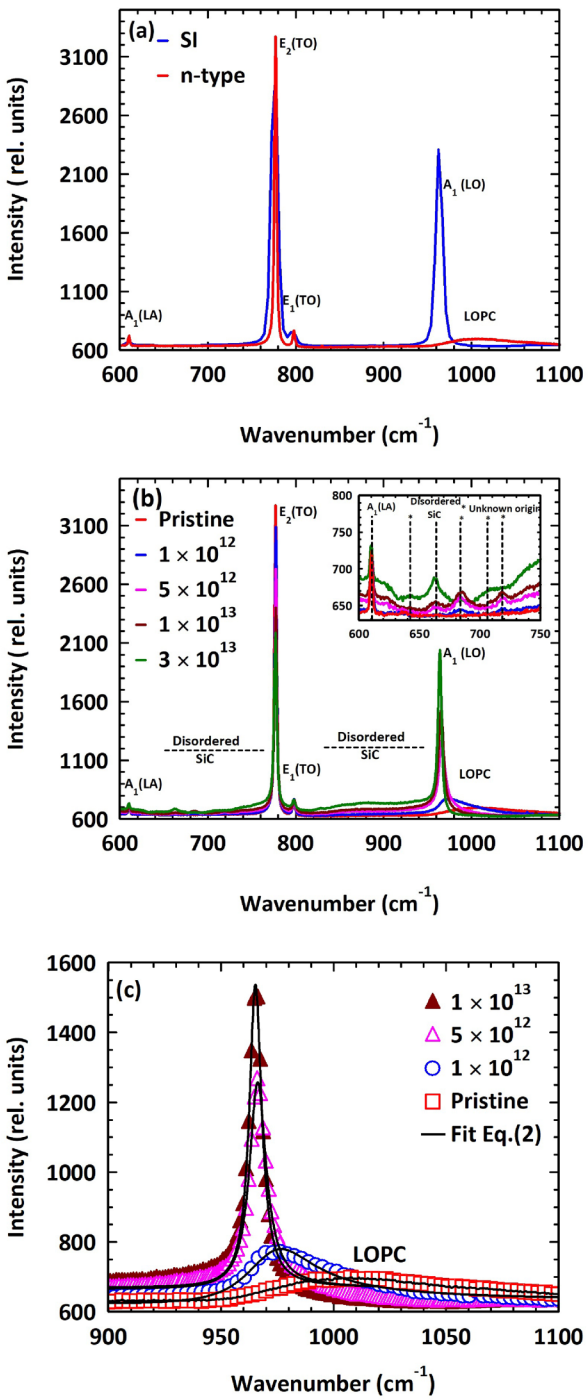

FIG. 3. (a) Raman spectra recorded on pristine semi-insulating and n-type 4H-SiC. (b) Raman spectra after 100 MeV Ag irradiation of n-type 4H-SiC with various fluences (ions/cm^2). Inset shows the zoomed view of the disordered SiC region (600–750 cm^{-1}) marked with prominent features of unknown origin. (c) LOPC decoupling from A_1(LO) (wavenumber range 900–1100 cm^{-1}) along with solid black lines corresponding to the fits to Eq. (2).

the characteristic Raman spectrum obtained for the pristine SI and n-type 4H-SiC samples. The spectra obtained on n-type 4H-SiC after Ag irradiations are presented in Fig. 3(b). The spectrum of the pristine samples shows various Raman-active modes of the hexagonal 4H-SiC structure, namely, the A_1, E_1, and E_2 modes that can be identified from previous reports.[23,50–55] Figure 3(b) clearly shows that the intensity of the most dominant mode [E_2(TO)] observed in the Raman spectrum of the pristine sample decreases as the irradiation fluence is increased. The spectrum also exhibits the longitudinal optical phonon–plasmon coupling (LOPC) mode near 1000 cm^{-1} originating from the interaction of free carriers (from n-type doping) with LO phonons.[23,51,52,54,55] The band consists of two components centered at 1001.93 and 1060.80 cm^{-1}. SHI irradiation results in a gradual shift to lower wavenumbers, and a narrowing of the LOPC mode [Fig. 3(c)]. The two bands eventually merge into a single narrow peak at around 964 cm^{-1}, which is assigned to the LO mode without coupling. The LOPC mode completely disappears upon irradiation with Ag fluence of 3×10^{13} ions/cm^2 and the peak center almost overlaps with the completely decoupled A_1 (LO) mode observed for the pristine SI 4H-SiC [Fig. 3(a)]. Further, a line shape analysis of the LOPC mode was carried out for the estimation of the free-carrier concentration as a function of irradiation fluence. The quantitative analysis of the carrier concentration was performed using the following fitting function:[56,57]

$$Intensity(\omega) \propto Amplitude(\omega) \times Im\left(\frac{-1}{\epsilon(\omega, q)}\right). \quad (1)$$

For simplicity, only the Brillouin zone center is considered and we assume that $q = 0$. Here, ω is the Raman frequency and $\epsilon(\omega)$ is the total dielectric function, including both electron and phonon contributions. $Amplitude(\omega)$ can be expressed as follows:

$$Amplitude(\omega) = 1 + B(\omega) + C(\omega), \quad (2)$$

where

$$B(\omega) = 2C_{fh}\frac{\omega_T^2}{\delta}[\omega_P^2\gamma_p(\omega_T^2 - \omega^2) - \omega^2\Gamma(\omega^2 + \gamma_p^2 - \omega_p^2)],$$

$$C(\omega) = \left(\frac{C_{fh}^2\omega_t^4}{\delta^*(\omega_L^2 - \omega_T^2)}\right)(\omega_P^2[\gamma_P(\omega_L^2 - \omega_T^2) + \Gamma(\omega_P^2 - 2\omega_2)] + \omega^2\Gamma(\omega^2 + \gamma_p^2)),$$

$$\delta = \omega_P^2\gamma_p((\omega_T^2 - \omega^2)^2 + \omega^2\Gamma^2) + \omega^2\Gamma(\omega_L^2 - \omega_T^2)(\omega_2 + \gamma_P^2),$$

where ω_L, ω_T, and ω_p are LO, TO, and plasmon frequencies, respectively, γ_p and Γ are the plasmon and phonon damping constants, respectively, and C_{fh} is the Faust–Henry coefficient.[58] The dielectric function $\epsilon(\omega)$ and the plasma frequency ω_p are given by the following equations:

$$\epsilon(\omega) = \epsilon_\infty\left(1 + \frac{\omega_L^2 - \omega_T^2}{\omega_T^2 - \omega^2 - i\omega^2\Gamma^2} - \frac{\omega_P^2}{\omega(\omega + i\gamma_P)}\right), \quad (3)$$

$$\omega_P^2 = \frac{4\pi ne^2}{\epsilon_0\epsilon_\infty m^*}, \quad (4)$$

where ϵ_∞ is the value of the dielectric function at high frequencies, m^* is the effective mass of electron, and n is the free-carrier concentration. The various parameters used for fitting are listed elsewhere.[57] The values of ω_p obtained after fitting the LOPC mode by Eqs. (1) and (2) for different irradiation fluences were used to estimate the carrier concentration n by Eq. (4). Hall measurements were performed on the samples and a good correlation was derived after comparing the Hall data with the LOPC Raman data. The parameters obtained from Raman and Hall measurements are presented in Table I.

Figure 4 shows that the variation of the normalized area under the A_1(LO)-plasmon decoupled band centered at around 964 nm, and the normalized carrier concentration derived using Hall measurements with irradiation fluence exhibits a single exponential growth-decay relationship. Similar values of the growth and decay cross sections suggest that the decoupling of the LOPC Raman band is closely related to a reduction in carrier concentration. This can be attributed to the trapping of the free carriers by defects increasing with irradiation fluence. The most probable electron trap centers generated after ion irradiation is the V_C as it has the lowest formation energy. Another possible defect that can be held responsible for trapping carriers is the V_{Si} with formation energy 3–4 eV higher than that of the V_C (see Ref. 2, and references therein).

The free-carrier concentration obtained from the Hall measurement is used to estimate the Burstein–Moss (BM) shift. The BM shift (Δ_{BM}) of the Fermi-level inside the conduction band as a result of states close to the conduction band edge being populated is estimated using the following relation:[87–89]

$$\Delta_{BM} = \frac{\hbar^2}{2m^*}(3\pi^2 n)^{\frac{2}{3}}, \quad (5)$$

TABLE I. Parameters derived using Eqs. (1)–(6) from Raman spectroscopy and Hall effect measurements on pristine and 100 MeV Ag irradiated n-type 4H-SiC.

100 MeV Ag Fluence (cm^{-2})	Fitting parameters		Raman measurements	Hall measurements		Burstein–Moss shift
	ω_P (cm^{-1})	γ (cm^{-1})	n (cm^{-3})	n (cm^{-3})	μ (cm^2/Vs)	Δ_{BM} (meV)
Pristine	549.03	887.87	6.50×10^{18}	6.78×10^{18}	59.63	48.7
1×10^{12}	418.83	1345.62	3.78×10^{18}	6.03×10^{18}	66.67	45.0
5×10^{12}	166.07	479.62	5.95×10^{17}	2.40×10^{17}	13	5.25
1×10^{13}	549.03	136.28	4.00×10^{17}	1.85×10^{17}	0.2	4.41
3×10^{13}	…	…	…	7.90×10^{16}	7.74×10^{-4}	2.50

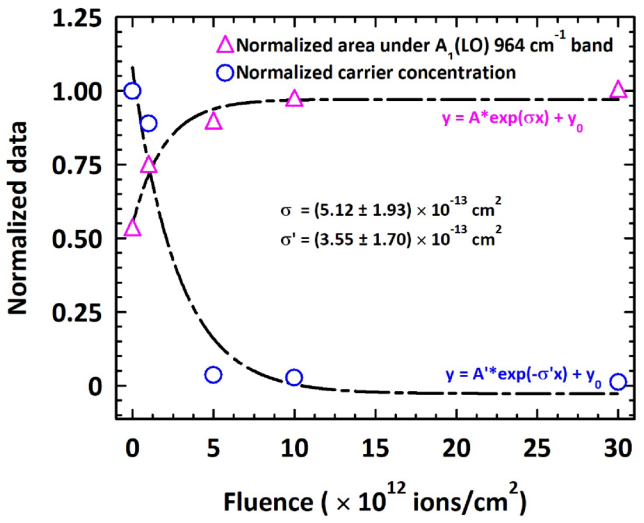

FIG. 4. Normalized area under the decoupled 964 cm^{-1} A_1 (LO) from longitudinal optical plasmon coupled (LOPC) Raman band and the normalized carrier concentration (Hall data) as a function of fluence for n-type 4H-SiC irradiated with 100 MeV Ag ions.

where $\hbar$ is the reduced Planck's constant, n is the free-carrier concentration, and m^* is the reduced effective mass of the charge carrier and it is expressed as[88]

$$m^* = \frac{m_n \times m_h}{m_n + m_h}. \quad (6)$$

Here, m_n and m_h are the effective masses of an electron and hole, respectively. $m_n = 0.39m_e$ and $m_h = 0.82m_e$ have been used in this study.[62] m_e is the mass of an electron. After irradiation, the Fermi-level tends to shift lower in energy as the fluence increases. Δ_{BM} estimated for the pristine sample is 48.7 meV considering the value of carrier concentration to be 6.78×10^{18} cm^{-3}. This value reduces to 2.5 meV for the sample irradiated using the highest fluence, indicating that the Fermi-level is still inside the conduction band.

C. UV-vis absorption spectroscopy

Normally, the absorption spectra of semiconductors are dominated by transitions from the valence band to the conduction band but the spectra can also show defect-related absorption bands below the fundamental bandgap. Figures 5(a) and 5(b) show the absorption spectra recorded on n-type and SI 4H-SiC after irradiation with SHI. The spectra obtained for the n-type 4H-SiC samples exhibit four distinct features: (i) band to band, (ii) band to donor level, (iii) inter-conduction band free-electron absorption, and (iv) absorption bands from the defect states,[63–67] whereas SI 4H-SiC samples only exhibit indirect allowed absorption transition in the region (i), allowing estimation of the bandgap energy (E_g) with fluence by fitting Tauc's equation.[68] The values of E_g shown in the inset of Fig. 5(c) suggest narrowing of the bandgap with

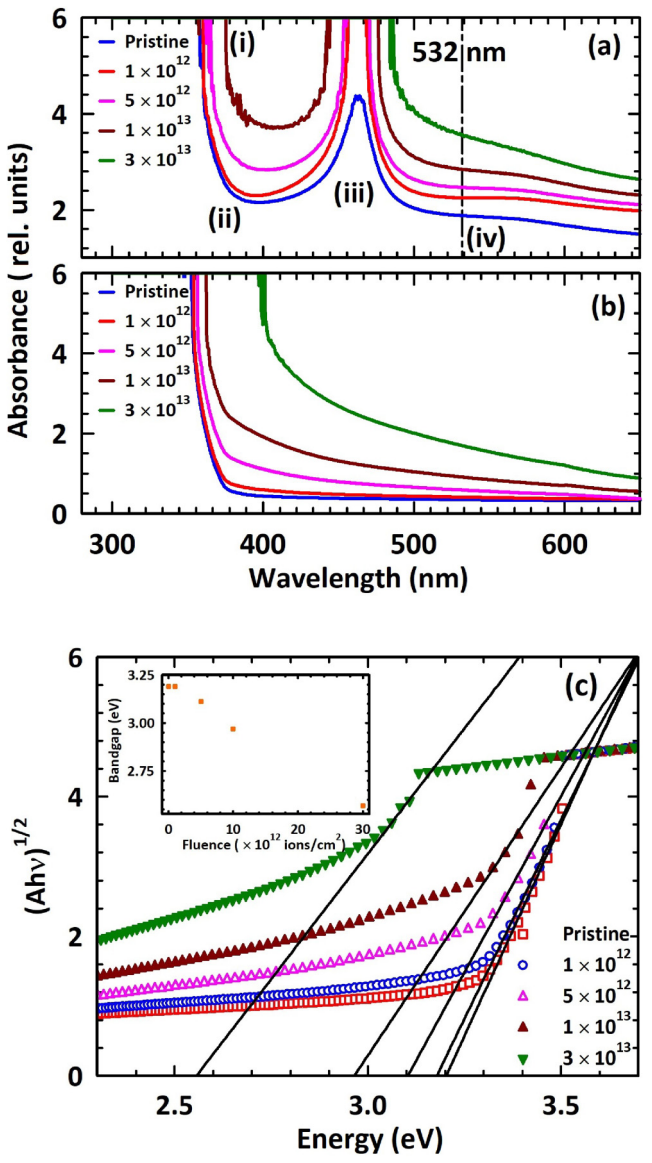

FIG. 5. Absorption spectra of pristine and 100 MeV Ag ion irradiated 4H-SiC at room temperature for various fluences (ions/cm^2): (a) n-type and (b) semi-insulating (SI). (c) Tauc-plot analysis indicating the indirect bandgap transition in SI 4H-SiC. Inset plot shows the variation of bandgap energy (E_g) determined in the region 3.20–2.50 eV at different Ag irradiation fluences.

increasing irradiation fluence. Bandgap engineering is required for quantum device design to stack diverse materials for quantum applications.[69] Photovoltaic solar cells have been using silicon carbide for decades.[70–76] Since the bandgap of SiC is more than what is required for effective solar energy absorption, Si rich SiC is grown with reduced bandgap leading to a substantial increase in absorption within the visible spectra.[77]

Narrowing of the bandgap with irradiation fluence can be attributed to the irradiation-induced, inhomogeneously distributed, ionized defects that exert opposite forces by Coulomb interactions with the carriers in the conduction and valence bands, leading to the formation of defect bands that tails into the bandgap along with the band edges.[78] A local mechanical strain that is produced due to the presence of defects after irradiation also plays a vital role in the alteration of the bandgap. It has been experimentally determined that energetic ion irradiations can induce significant lattice strain in SiC.[79–82] In Fig. 5(a), as compared to the SI 4H-SiC, the N-doping in n-type 4H-SiC leads to a drastic modification in the visible range of the absorption spectra due to the presence of shallow donors.[83] In the below bandgap region, an absorption peak at a wavelength of about 463 nm is observed in n-type 4H-SiC, which is associated with the free-carrier absorption transitions between the set of conduction subbands (M to Γ transition/c1 to c4 transition at M point).[64–66,84] To enable evaluation of the nitrogen concentration from the absorption at 463 nm, an empirical relation was proposed by Weingärtner *et al.*[85,86] The function predicts a linear relationship between nitrogen donor concentration and absorbance. Contrastingly, our results show that there is an enhancement of absorption at 463 nm even when there is a decrease in free-carrier concentration with increasing irradiation fluence. This indicates that there is a role of ion beam-induced defects in the enhancement of absorption in this region. In a recent experimental work, after Gamma irradiation of n-type 4H-SiC, the absorbance of this transition enhanced and reached the detector saturation limit along with an increase in the bandgap disorder as the Gamma dose was increased.[67] In our case, similar observations are made regarding the evolution of the absorbance related to this inter-conduction band transition with increasing irradiation fluence. We observe exceptionally high absorption at 463 nm as compared to the overall below bandgap absorption in the samples irradiated using 1×10^{12} ions/cm^2 relative to the unirradiated samples. Band to band absorption [region (i) in Fig. 5(a)] of these two samples nearly overlap, showing insignificant band edge narrowing due to the formation of tail state. The number of defects that are created due to irradiation is $\sim 10^{19}$ cm^{-3}. This seems to be the reason for this enhancement of the inter-conduction band transitions and below bandgap absorptions. These isolated defects, mostly vacancy type, are expected to act as free-electron traps. V_C and V_{Si} are known to form defect states within the bandgap. In n-type 4H-SiC, these defects are anticipated to capture free electrons from the conduction band and remain in the negatively charged state.[2,87–89] The photoabsorption by these trapped electrons results in excitation to the conduction band, enhancing the below bandgap absorption. However, this cannot explain the enhanced inter-conduction band transitions as the free-carrier concentration remains almost unchanged in these two samples. One possibility may be that shallow electron traps are formed from which electrons are excited to the C_4 conduction sub-band by photoabsorption.

Further analysis established a correlation between the decrease in intensity of the E_2(TO) Raman mode, and absorption by defect centers with increasing irradiation fluence. Evolution of the normalized absorbance along the 532 nm (defect-related absorption) wavelength same as the Raman laser wavelength, and normalized area under the E_2(TO) with irradiation fluence indicated a relationship between Raman and absorption as previously predicted in the literature.[50] Fitting using exponential growth and decay functions, similar cross-section values were obtained for both (Fig. 6), suggesting that the evolution of the E_2(TO) Raman bands is closely related to the presence of defects acting as strong absorbing centers.

Finally, a comparison is made between the normalized vacancy concentration evaluated from Fig. 1(b), and the absolute change in the normalized values of the E_g, area under E_2(TO) Raman mode, and carrier concentration after irradiation with various fluences. It can be seen from Fig. 7 that the absolute change (decrease) in the normalized bandgap energy with fluence evolves in a much slower rate as compared to the vacancy production. This gives rise to a speculation that some of the vacancy-interstitial pairs that are created by the SHI must have been consequently annealed by ionization-induced self-healing. The SHI induced thermal spike results in high lattice temperatures above which vacancy migration is enhanced and can be considered as the mechanism to justify the self-annealing of defects. We have recently reported that thermal spike due to 100 MeV Ag can recrystallize predamaged SiC even at room temperature.[24] This explanation also supports the lower rate of change (decrease) in the normalized area under E_2(TO) Raman mode as compared to the growth rate of vacancies. Interestingly, the value of the absolute change (decrease) in normalized carrier concentration exhibits a sudden jump as the irradiation fluence varies from 1×10^{12} to 5×10^{12} ions/cm^2. As the fluence is further increased, this value remains almost unchanged. Here, it can be conjectured that a significant concentration of trap centers is produced until the irradiation fluence of 5×10^{12} ions/cm^2; beyond that, the defects produced may not be electron traps. We also observed that V_{Si} related PL emission starts decreasing beyond this fluence.

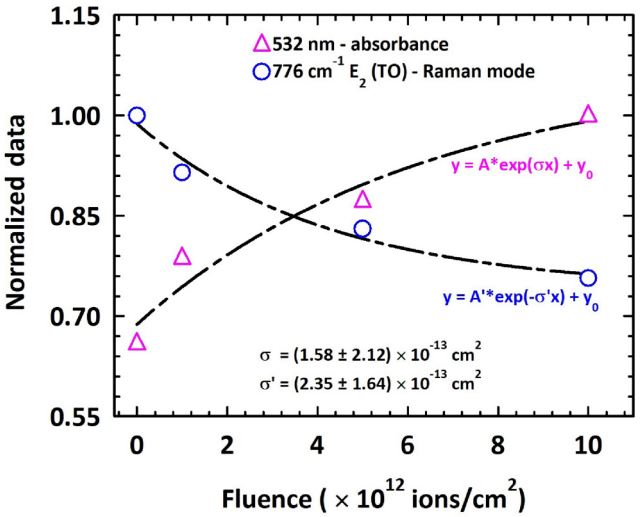

FIG. 6. Normalized absorbance at 532 nm (same wavelength as Raman source) and the normalized intensity of the 776 cm^{-1} (E_2(TO)) Raman band as a function of fluence for n-type 4H-SiC irradiated with 100 MeV Ag ions.

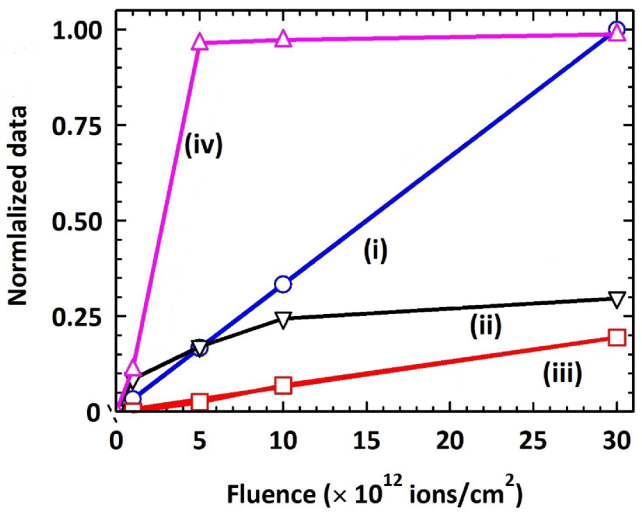

FIG. 7. Normalized data vs fluence for 100 MeV Ag irradiation in 4H-SiC. The data includes (i) normalized vacancy concentration predicted using TRIM,[22] (ii) 1-normalized area under E_2(TO) Raman mode, (iii) 1-normalized values of the bandgap, and (iv) 1-normalized values of the carrier concentration, taken from Hall data in Table I.

IV. CONCLUSION

The capability of swift heavy ions (SHI) to produce uniform defect concentrations within a considerable volume of materials has been utilized to achieve micrometers deep uniform defect depth profiles. Using Monte-Carlo based TRIM simulation, it is shown that these defects are uniformly distributed within a sample depth of approximately 5 μm. This opens up a method for the production of uniform vacancy distribution within several micrometers. From photoluminescence measurement, it is established that technologically important V_{Si} defects can be populated by 100 MeV Ag irradiation. Further experimental probing of the samples indicates decoupling of the LOPC Raman mode due to the trapping of the free carriers by defects. This is consistent with the decreasing values of carrier concentration with fluence as obtained from Hall measurements and LOPC fitting. The observed reduction in the intensity of the dominant Raman mode is attributed to the enhanced optical absorption due to the presence of defects acting as strong absorbing centers. The appearance of disordered Si–C bands is associated with the breakdown of the Raman selection rules induced by the accumulation of point defects. The narrowing of the optical bandgap with irradiation fluence is attributed to the formation of localized tail states in the forbidden gap. The enhanced inter-conduction band transitions are linked to an increase in the trap centers with irradiation and subsequent photo-excitation of the trapped electrons to a higher conduction sub-band.

ACKNOWLEDGMENTS

A.C. would like to acknowledge the Council of Scientific and Industrial Research (CSIR), India for financial support through fellowship. B.S. acknowledges the Department of Science and Technology of India for a Fellowship and Research Grant under the DST-INSPIRE Faculty award program (No. IFA14-PH-109). D. Kanjilal is thankful to DAE BRNS for the Raja Ramanna Fellowship. The authors are thankful to the Pelletron group at IUAC, New Delhi.

DATA AVAILABILITY

The data that support the findings of this study are available from the corresponding author upon reasonable request.

REFERENCES

[1]H. Abderrazak and E. S. B. H. Hmida, *Silicon Carbide: Synthesis and Properties, Properties and Applications of Silicon Carbide*, edited by R. Gerhardt (IntechOpen, 2011), pp. 361–388.
[2]N. Iwamoto and B. G. Svensson, *Defects in Semiconductors, Point Defects in Silicon Carbide*, edited by L. Romano, V. Privitera, and C. Jagadish (Elsevier, 2015), pp. 369–407.
[3]K. Nordlund, S. J. Zinkle, A. E. Sand, F. Granberg, R. S. Averback, R. E. Stoller, T. Suzudo, L. Malerba, F. Banhart, W. J. Weber, F. Willaimei, S. L. Dudarev, and D. Simeone, J. Nucl. Mater. **512**, 450 (2018).
[4]K. Nordlund, S. J. Zinkle, A. E. Sand, F. Granberg, R. S. Averback, E. Stoller, T. Suzudo, L. Malerba, F. Banhart, W. J. Weber, F. Willaimei, S. L. Dudarev, and D. Simeone, Nat. Commun. **9**, 1084 (2018).
[5]W. F. Koehl, B. B. Buckley, F. J. Heremans, G. Calusine, and D. D. Awschalom, Nature **479**, 84–87 (2011).
[6]A. L. Falk, B. B. Buckley, G. Calusine, W. F. Koehl, V. V. Dobrovitski, A. Politi, and D. D. Awschalom, Nat. Commun. **4**, 1819 (2013).
[7]S. Castelletto, B. C. Johnson, V. Ivády, N. Stavrias, T. Umeda, A. Gali, and T. Ohshima, Nat. Mater. **13**, 151 (2014).
[8]S. Castelletto, B. C. Johnson, C. Zachreson, D. Beke, I. Balogh, T. Ohshima, I. Aharonovich, and A. Gali, ACS Nano **8**, 7938 (2014).
[9]J. F. Wang, Y. Zhou, Z. Y. Wang, A. Rasmita, J. Q. Yang, X. Li, H. J. V. Bardeleben, and W. Gao, Nat. Commun. **9**, 631 (2018).
[10]A. Lohrmann, N. Iwamoto, Z. Bodrog, S. Castelletto, T. Ohshima, T. J. Karle, A. Gali, S. Prawer, J. C. McCallum, and B. C. Johnson, Nat. Commun. **6**, 1009 (2015).
[11]D. J. Christle, A. L. Falk, P. Andrich, P. V. Klimov, J. U. Hassan, N. T. Son, E. Janzén, T. Ohshima, and D. D. Awschalom, Nat. Mater. **14**, 160 (2015).
[12]M. Widmann, S. Y. Lee, T. Rendler, N. T. Son, H. Fedder, S. Paik, L. Yang, N. Zhao, S. Yang, I. Booker, A. Denisenko, M. Jamali, S. A. Momenzadeh, I. Gerhardt, T. Ohshima, A. Gali, E. Janzén, and J. Wrachtrup, Nat. Mater. **14**, 164 (2015).
[13]P. G. Baranov, A. P. Bundakova, A. A. Soltamova, S. B. Orlinskii, I. V. Borovykh, R. Zondervan, R. Verberk, and J. Schmidt, Phys. Rev. B **83**, 125203 (2011).
[14]F. Fuchs, B. Stender, M. Trupke, D. Simin, J. Pflaum, V. Dyakonov, and G. V. Astakhov, Nat. Commun. **6**, 204 (2015).
[15]H. Kraus, V. Soltamov, F. Fuchs, D. Simin, A. Sperlich, P. Baranov, G. Astakhov, and V. Dyakonov, Sci. Rep. **4**, 5303 (2014).
[16]A. N. Anisimov, D. Simin, V. A. Soltamov, S. P. Lebedev, P. G. Baranov, G. V. Astakhov, and V. Dyakonov, Sci. Rep. **6**, 33301 (2016).
[17]H. Kraus, V. A. Soltamov, D. Riedel, S. Väth, F. Fuchs, A. Sperlich, P. G. Baranov, V. Dyakonov, and G. V. Astakhov, Nat. Phys. **10**, 157–162 (2014).
[18]R. Nagy, M. Widmann, M. Niethammer, D. B. Dasari, I. Gerhardt, Ö. O. Soykal, M. Radulaski, T. Ohshima, J. Vučković, N. T. Son, I. G. Ivanov, S. E. Economou, C. Bonato, S. Y. Lee, and J. Wrachtrup, Phys. Rev. Appl. **9**, 034022 (2018).

[19]J. F. Wang, X. M. Zhang, Y. Zhou, K. Li, Z. Y. Wang, P. Peddibhotla, F. C. Liu, S. Bauerdick, A. Rudzinski, Z. Liu, and W. B. Gao, ACS Photonics **4**(5), 1054 (2017).
[20]J. Achard, V. Jacques, and A. Tallaire, J. Phys. D: Appl. Phys. **53**, 313001 (2020).
[21]J. M. Smith, S. A. Meynell, A. C. Bleszynski Jayich, and J. Meijer, Nanophotonics **8**(11), 1889 (2019).
[22]J. F. Ziegler, M. D. Ziegler, and J. P. Biersack, Nucl. Instrum. Methods Phys. Res. Sect. B **268**, 1818 (2010).
[23]A. Chakravorty, B. Singh, H. Jatav, S. Ojha, J. Singh, D. Kanjilal, and D. Kabiraj, J. Appl. Phys. **128**, 165901 (2020).
[24]B. Zippelius, J. Suda, and T. Kimoto, J. Appl. Phys. **111**, 033515 (2012).
[25]L. Heyi, C. Liu, Y. Zhang, C. Qi, Y. Wei, J. Zhou, T. Wang, G. Ma, Z. Wang, S. Dong, and M. Huo, Semicond. Sci. Technol. **34**, 095010 (2019).
[26]D. Kanjilal, S. Chopra, M. M. Narayanan, I. S. Iyer, V. Jha, R. Joshi, and S. K. Datta, Nucl. Instrum. Methods Phys. Res. Sect. A **328**, 97 (1993).
[27]T. A. G. Eberlein, C. J. Fall, R. Jones, P. R. Briddon, and S. Öberg, Phys. Rev. B **65**, 184108 (2002).
[28]M. Bockstedte, A. Gali, A. Mattausch, O. Pankratov, and J. W. Steeds, Phys. Status Solidi B **245**, 1281 (2008).
[29]V. Kozlovski and V. Abrosimova, *Radiation Defect Engineering Selected Topics in Electronics and Systems* (World Scientific, Singapore, 2005), Vol. 37.
[30]E. Janzén, A. Gali, P. Carlsson, A. Gällström, B. Magnusson, and N. T. Son, Physica B **404**, 4354–4358 (2009).
[31]T. Egilsson, J. P. Bergman, I. G. Ivanov, A. Henry, and E. Janzén, Phys. Rev. B **59**, 1956 (1999).
[32]A. Gali, P. Deák, E. Rauls, N. T. Son, I. G. Ivanov, F. H. C. Carlsson, E. Janzén, and W. J. Choyke, Phys. Rev. B **67**, 155203 (2003).
[33]T. A. G. Eberlein, R. Jones, S. Öberg, and P. R. Briddon, Phys. Rev. B **74**, 144106 (2006).
[34]G. Li, L. W. Burggraf, J. R. Shoemaker, D. Eastwood, and A. E. Stiegman, Appl. Phys. Lett. **76**, 3373 (2000).
[35]X. Liu, L. Cao, H. Song, and H. Jiang, Physica E **61**, 167–170 (2014).
[36]J. Renxu, Z. Yimen, Z. Yuming, W. Yuehu, and Z. Lin, J. Semicond. **30**, 033003 (2009).
[37]A. N. Andreev, M. M. Anikin, A. A. Lebedev, N. K. Poletaev, A. M. Strel'chuk, A. L. Syrkin, and V. E. Chelnokov, Semiconductors **28**, 430 (1994); available at https://ui.adsabs.harvard.edu/abs/1994Semic..28..430A/abstract.
[38]A. A. Lebedev, B. Y. Ber, N. V. Seredova, D. Y. Kazantsev, and V. V. Kozlovski, J. Phys. D **48**, 485106 (2015).
[39]V. V. Kozlovski, A. A. Lebedev, E. V. Bogdanova, and N. V. Seredova, Semiconductors **49**, 1163 (2015).
[40]E. V. Kalinina, N. A. Chuchvaga, E. V. Bogdanova, A. M. Strel'chuk, D. B. Shustov, M. V. Zamoryanskaya, and V. A. Skuratov, Semiconductors **48**, 156 (2014).
[41]N. I. Morozov and D. I. Tetelbaum, Sov. Phys. Semicond. **17**, 524 (1983); available at https://scholar.google.com/scholar_lookup?title=&journal=Sov.%20Phys.%20Semicond.&volume=17&publication_year=1983&author=Morozov%2CN%20I&author=Tetelbaum%2CD%20I.
[42]P. V. Pavlov, Yu. A. Semin, and V. D. Skupov, Sov. Phys. Semicond. **20**, 315 (1986); available at http://pascal-francis.inist.fr/vibad/index.php?action=getRecordDetail&idt=7908059.
[43]E. V. Kolesnikova, E. V. Kalinina, A. A. Sitnikova, M. V. Zamoryanskaya, and T. B. Popova, Solid State Phenom. **131–133**, 53 (2008).
[44]E. V. Kalinina, M. V. Zamoryanskaya, E. V. Kolesnikova, and A. A. Lebedev, Mater. Sci. Forum **615–617**, 473–476 (2009).
[45]D. B. Shustov, E. V. Kolesnikova, E. V. Kalinina, V. A. Skuratov, and M. V. Zamoryanskaya, Solid State Phenom. **156–158**, 401 (2010).
[46]V. A. Perevoshchikov and V. D. Skupov, *Gettering Impurities and Defects in Semiconductors* (Nizhegorod State University, Nizhni Novgorod, 2002), Pt. 1, Chap. 3, p. 158 (in Russian).
[47]M. Rühl, C. Ott, S. Götzinger, M. Krieger, and H. B. Weber, Appl. Phys. Lett. **113**, 122102 (2018).
[48]D. Riedel, F. Fuchs, H. Kraus, S. Väth, A. Sperlich, V. Dyakonov, A. A. Soltamova, P. G. Baranov, V. A. Ilyin, and G. V. Astakhov, Phys. Rev. Lett. **109**, 226402 (2012).
[49]S. Sato, T. Narahara, Y. Abe, Y. Hijikata, T. Umeda, and T. Ohshima, J. Appl. Phys. **126**, 083105 (2019).
[50]S. Sorieul, J.-M. Costantini, L. Gosmain, L. Thomé, and J.-J. Grob, J. Condens. Matter Phys. **18**, 5235 (2006).
[51]J. C. Burton, L. Sun, M. Pophristic, S. J. Lukacs, F. H. Long, Z. C. Feng, and I. T. Ferguson, J. Appl. Phys. **84**, 6268 (1998).
[52]J. C. Burton, L. Sun, F. H. Long, Z. C. Feng, and I. T. Ferguson, Phys. Rev. B **59**, 7282 (1999).
[53]S. Nakashima and H. Harima, Phys. Status Solidi A **162**, 39 (1997).
[54]S. Nakashima, T. Kitamura, T. Mitani, H. Okumura, M. Katsuno, and N. Ohtani, Phys. Rev. B **76**, 245208 (2007).
[55]S. Sorieul, X. Kerbiriou, J.-M. Costantini, L. Gosmain, G. Calas, and C. Trautmann, J. Condens. Matter Phys. **24**, 125801 (2012).
[56]G. Irmer, M. Wenzel, and J. Monecke, Phys. Rev. B **56**, 9524 (1997).
[57]M. Chafai, A. Jaouhari, A. Torres, R. Antón, E. Martín, J. Jiménez, and W. C. Mitchel, J. Appl. Phys. **90**, 5211 (2001).
[58]W. L. Faust and C. H. Henry, Phys. Rev. Lett. **17**, 1265 (1966).
[59]E. F. Schubert, *Doping in III–V Semiconductors*, edited by H. Ahmed, M. Pepper, and A. Broers (Cambridge University Press, 1993), digitally printed first paperback version 2005, pp. 37–79.
[60]S. Gahlawat, J. Singh, A. K. Yadav, and P. P. Ingole, Phys. Chem. Chem. Phys. **21**(36), 20463-–20477 (2019).
[61]B. Singh, Z. Ahmed Khan, I. Khan, and S. Ghosh, Appl. Phys. Lett. **97**, 241903 (2010).
[62]T. Ayalew, "SiC semiconductor devices technology, modeling, and simulation," Doctoral dissertation (Vienna University of Technology, Faculty of Electrical Engineering and Information Technology, Austria, 2004), see https://www.iue.tuwien.ac.at/phd/ayalew/node62.html.
[63]E. Biedermann, Solid State Commun. **3**, 343–346 (1965).
[64]C. Persson and U. Lindefelt, J. Appl. Phys. **82**, 5496 (1997).
[65]S. Limpijumnong, W. R. L. Lambrecht, S. N. Rashkeev, and B. Segall, Phys. Rev. B **59**, 12890 (1999).
[66]S. Zollner, J. G. Chen, E. Duda, T. Wetteroth, S. R. Wilson, and J. N. Hilfiker, J. Appl. Phys. **85**, 8353 (1999).
[67]I. P. Vali, P. K. Shetty, M. G. Mahesha, V. G. Sathe, D. M. Phase, and R. J. Choudhary, Nucl. Instrum. Methods Phys. Res. Sect. B **440**, 101 (2019).
[68]J. Tauc, *Amorphous and Liquid Semiconductors* (Springer US, 1974), p. 170.
[69]J. Bao, Nat. Nanotechnol. **10**, 19–20 (2015).
[70]J. W. Sun, V. Jokubavicius, L. Gao, I. Booker, M. Jansson, X. Y. Liu, J. P. Hofmann, E. J. M. Hensen, M. K. Linnarsson, P. J. Wellmann, I. Ramiro, A. Martí, R. Yakimova, and M. Syväjärvi, Mater. Sci. Forum **858**, 1028–1031 (2016).
[71]Y. C. Tsai, M. Y. Lee, Y. Li, M. M. Rahman, and S. Samukawa, IEEE Electron. Device Lett. **37**, 758–761 (2016).
[72]I. A. Yunaz, K. Hashizume, S. Miyajima, A. Yamada, and M. Konagai, Sol. Energy Mater. Sol. Cells **93**, 1056–1061 (2009).
[73]M. Konagai, Thin Solid Films **516**, 490–495 (2008).
[74]S. Miyajima, K. Haga, A. Yamada, and M. Konaga, Jpn. J. Appl. Phys. **45**, L432–L434 (2006).
[75]R. P. Raffaelle, N. York, S. G. Bailey, P. Neudeck, R. Okojie, N. Glenn, C. M. Schnabel, and C. Western, "Optical and electrical of SiC devices," in *Conference Record of the Twenty-Eighth IEEE Photovoltaic Specialists Conference—2000 (Cat. No. 00CH37036)* (IEEE, 2000), pp. 1257–1260.
[76]Y. Tawada, H. Okamoto, and Y. Hamakawa, Appl. Phys. Lett. **39**, 237–239 (1981).
[77]N. D. Alkhaldi, S. K. Barman, and M. N. Huda, Heliyon **5**, e02908 (2019).
[78]J. I. Pankove, *Optical Processes in Semiconductors* (Dover Publications, Inc., New York, 1975), unabridged republication of the work originally published by Prentice-Hall, Inc., 1971, pp. 10–11.
[79]F. X. Zhang, Y. Tong, H. Xue, J. K. Keum, Y. Zhang, A. Boulle, A. Debelle, and W. J. Weber, Appl. Phys. Lett. **114**, 221904 (2019).

[80]A. Debelle, L. Thomé, D. Dompoint, A. Boulle, F. Garrido, J. Jagielski, and D. Chaussende, J. Phys. D: Appl. Phys. **43**, 455408 (2010).
[81]A. Debelle, A. Boulle, A. Chartier, F. Gao, and W. J. Weber, Phys. Rev. B **90**, 174112 (2014).
[82]A. Boulle, A. Debelle, J. B. Wallace, L. B. Bayu Aji, and S. O. Kucheyev, Acta Mater. **140**, 250–257 (2017).
[83]A. O. Evwaraye, S. R. Smith, and W. C. Mitchel, J. Appl. Phys. **79**, 7726 (1996).
[84]Y. Fang, X. Wu, J. Yang, G. Chen, Y. Chen, Q. Wu, and Y. Song, Appl. Phys. Lett. **112**, 201904 (2018).
[85]R. Weingärtner, P. J. Wellmann, M. Bickermann, D. Hofmann, T. L. Straubinger, and A. Winnacker, Appl. Phys. Lett. **80**, 70 (2002).
[86]D. D. Firsov, S. Komkov, A. Y. Fadeev, and A. O. Lebedev, J. Phys.: Conf. Ser. **741**, 012043 (2016).
[87]X. Wang, J. Zhao, Z. Xu, F. Djurabekova, M. Rommel, Y. Song, and F. Fang, Nanotechnol. Precis. Eng. **3**, 211-217 (2020).
[88]J. Coutinho, Crystals **11**, 167 (2021).
[89]M. E. Bathen, A. Galeckas, J. Müting, H. M. Ayedh, U. Grossner, J. Coutinho, Y. K. Frodason, and L. Vines, npj Quantum Inf. **5**, 111 (2019).